A Lumped-Parameter Model of a Smart Ventilation unit for nearly Zero Energy Buildings

A Lumped-Parameter Model of a Smart Ventilation unit for nearly Zero Energy Buildings

R Sedoni[1,*], G Cannistraci[4], P E Santangelo[1,2], D Angeli[1,3], M Romani[4], L Fioravanti[4]

[1] DISMI - Dipartimento di Scienze e Metodi dell'Ingegneria, Università degli Studi di Modena e Reggio Emilia, Reggio Emilia (Italy)
[2] Centro interdipartimentale per la ricerca InterMech – MO.RE., Modena (Italy)
[3] Centro Interdipartimentale En&Tech, Reggio Emilia (Italy)
[4] Zehnder Group – Competence Center Campogalliano, Campogalliano (Italy)

* Corresponding author: 225791@studenti.unimore.it

Abstract. In the present work, a simple model of a ventilation unit used for residential purposes is proposed, which was developed by means of MATLAB Simulink and the Simscape toolbox, also including the Moist Air and Two-Phase fluid libraries. This study falls in the realm of air conditioning in nearly Zero Energy Buildings. The model presented here is focused mostly on the aeraulic system. A parametric analysis of various installation conditions was conducted to assess and enhance the combined heat pump and the air distribution system performance, under various operating conditions. Therefore, the overall approach included several parameters, such as outdoor and indoor air temperature, humidity, static pressure, pressure drop in the intake and the distribution ducts, and filter fouling. The model serves as a predictive tool to evaluate the effectiveness of the whole system, in both design and off-design conditions; notably, critical conditions are emphasized, which are associated to severe fouling conditions, making the use of an additional fan ineffective.

Keywords: lumped-parameter model, multifunctional unit, moisture transport, mechanical ventilation, filter fouling

1. Introduction

Currently, HVAC (Heating, Ventilation and Air Conditioning) systems have assumed a critical role in ensuring optimal indoor air quality, thermal comfort, and energy efficiency in buildings. As the emphasis on sustainability and energy saving continues to grow, there is an increasing demand for enhancing HVAC systems and their efficiency. HVAC systems are known to consume a significant amount of energy within buildings, and their inefficient operation leads to energy wast, increased carbon emissions and energy expenses [1]. Consequently, the pursuit of improving the efficiency of HVAC systems has emerged as a significant area of research.

As available in the open literature, researchers dedicated considerable efforts to the development of simple analytical models aimed at examining fundamental components of air treatment systems. Among these components, the enthalpy recovery exchanger, which plays a vital role, has received substantial attention [2, 3]. Further studies have explored the diffusivity characteristics of permeable membranes within these exchangers [4, 5].

Moreover, investigations have been carried out to analyze the impact of specific boundary conditions on the performance of standard ventilation units. Manz et al. [6] delved into the performance evaluation of a single room ventilation unit employing either recuperative or regenerative heat recovery exchangers. Meanwhile, Filis et al. [7] examined the influence of wind pressure and stack effect on total sensible heat recovery and supply air temperatures.

However, there is currently no simple modeling approach able to take into account all the possible external/internal effects to which a HVAC system may be subjected, as well as to observe the response of its control logic to these effects.

The present study features a comprehensive analysis of ad hoc developed HVAC unit for nZEB (nearly Zeb Energy Builindgs), through a simple approach that can considers all the relevant effects impacting on the system performance. For this purpose a new Simscape block for the Moist Air library was devised and implemented to model the energy recovery (enthalpy) heat exchangers. The study provides a deep insight into the crucial aspects connected to the inclusion of an additional fan aimed at improving the unit performance.

2. System description

The considered system integrates a well-balanced mass/volume flow ventilation unit with an air-to-air heat pump (HP), with the aim of optimizing energy consumption and delivering thermal comfort in residential buildings. Unlike conventional products, this system operates in a distinct manner. The ventilation unit works within a flow rate range of 0 to 450 m^3 h^{-1}, while the heat pump unit operates with a balanced volume flow rate varying from 0 to 600 m^3 h^{-1}, thanks to the inclusion of a third fan (OEA) in the heat pump unit. The outdoor air (ODA) is extracted from the surroundings using the ventilation unit fan and is subsequently directed through the heat pump ducts, pre-heater, energy recovery ventilation (ERV) or heat recovery ventilation (HRV) heat exchanger, and the evaporator or condenser heat exchanger of the heat pump. The resulting supply air (SUP) flow is then conveyed to the target environment. A different part of the circuit handles the extracted air (ETA) from the internal environment, which is expelled outdoors (exhaust air EHA), after its passage through the ERV or HRV and the heat exchanger of the HP. To enhance the heat transfer rate at the evaporator (during heating season) or condenser (during cooling season), a third fan has been incorporated in the heat pump. This fan extracts air from the outside through the supply duct and propels it directly into the EHA duct upstream of the heat exchanger via a bypass line, thereby boosting the volume flow rate of EHA. It is essential to note that the OEA fan operates within specific limits, including a maximum revolution speed of 2500 rpm and restricted dimensions. These limitations were implemented to satisfy the design requirement of reducing and controlling noise levels, ultimately ensuring the acustic comfort of the occupants. A comprehensive schematic representation of the aeraulic circuit system is illustrated in Figure 1.

3. Model development

3.1. Aeraulic circuit

With regards to the aeraulic side of the circuit, the pressure losses of the singular components that composes the circuit (such as air ducts, filters, check valve, ERV/HRV, and T-junctions) are estimated using the known relationship:

$$\Delta p = R\dot{m}^2 \tag{1}$$

where R is the specific resistance of the component, and $\dot{m}$ is the mass flow through the component. The values of R are for the most obtained from the technical data sheets of components.

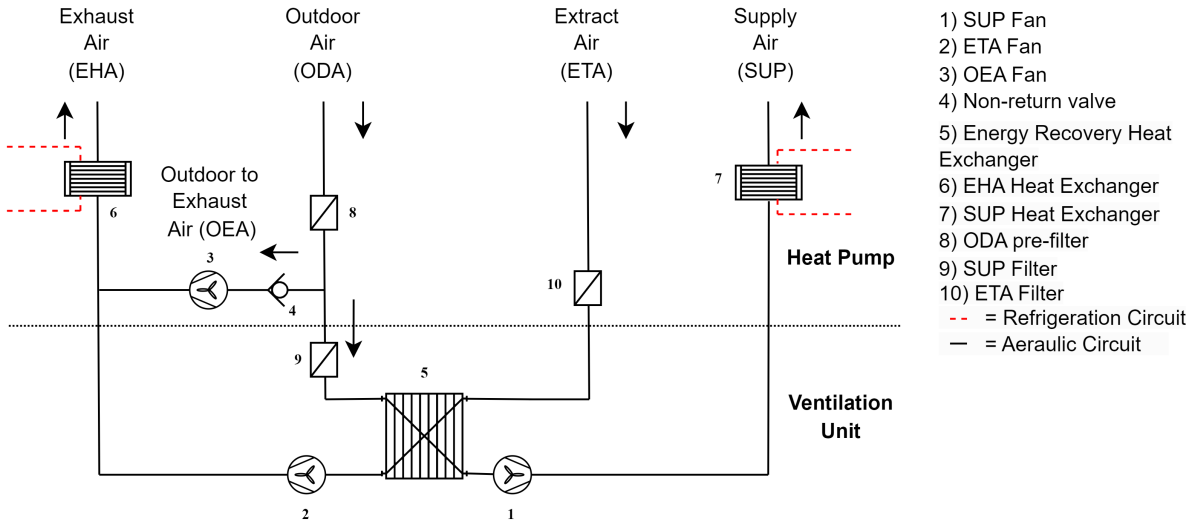

Figure 1. Aeraulic circuit of the unit investigated

The heat pump exchangers (EHA and SUP) analyzed are commercial cross-flow fin-type heat exchangers, which can be easily and accurately represented using the pre-defined "Condenser-Evaporator (2P-MA)" [8] block in Simscape. In this case, the air-side pressure drops are automatically calculated from the geometric characteristics of the heat exchanger.

With the technical data sheets of the fans available, it is possible to use the specific block "Fan (MA)" [8] for a detailed representation of the pressure gain provided by the fans to the air. Through this block, it is possible to specify a nominal operating condition and obtain from it a dimensionless scaling of the characteristic operating curves using the fan laws.

3.2. Energy recovery exchanger model

An ERV is an air-to-air heat exchanger that transfers both temperature and moisture, while a HRV can only transfer sensible heat. The system cools and dehumidifies outside air during the cooling season by sending excess heat and moisture into the exhaust airstream; this in turn cools the condenser coil down to lower temperature. During the heating season, the system pre heats and humidifies incoming air by conveying heat and moisture from the exhaust airstream, resulting in the exhaust air being cooler during the cooling season and warmer during the heating season.

These types of heat exchangers typically consist of a series of rectangular ducts that primarily operate in a counterflow configuration. Nonetheless (see Figure 2 a), a small part of the exchanger is configured in cross-flow mode. However, focusing only on the counterflow section for evaluating the exchange characteristics results in a negligible error.

The overall effectiveness of the exchanger varies depending on the geometric configuration of the channels and the physical characteristics of the membrane. The main channel configurations currently available in the market are Vertical Flat Panel, Horizontal Flat Panel, and Cellular. The latter structure (fig. 2 b) is generally the most efficient in terms of effectiveness and is the one used by the system analyzed in this work.

A pre-existing heat exchanger model with the exact specifications required is not readily available in Simscape. Therefore it was needed to rebuild it starting from the base block, i.e. 'Pipe (MA)' [8]. This is nothing more than a component of an air circuit in which it is possible to foresee an exchange of heat and moisture with the outside environment.

The main idea underlying the current modeling approach is to impose heat and moisture

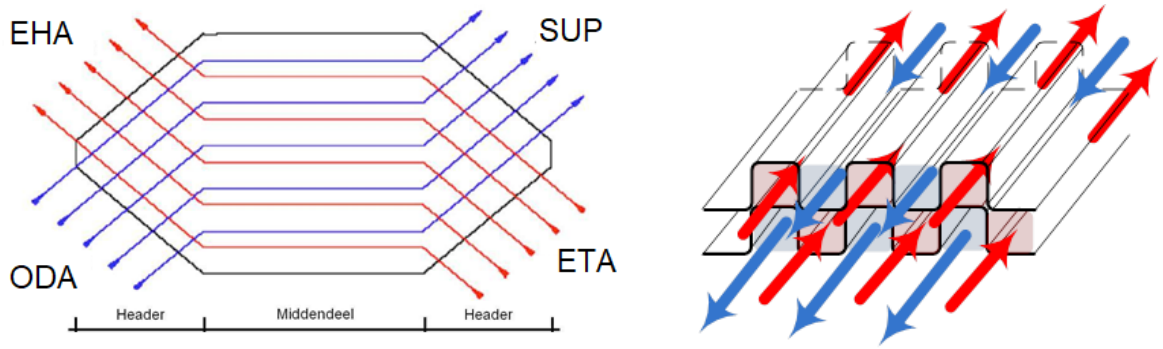

(a) Flow arrangement (b) Cellular structure

Figure 2. ERV/HRV Exchanger

transfer between the two streams through the thermal energy and moisture conserving ports of the Pipe (MA) blocks.

To finalize the modeling, two by-pass lines were added in parallel with the exchange lines of the heat exchanger. These are used to replicate the free flow area within the heat exchanger, where heat and humidity transfer is negligible. Additionally, the by-pass control logic is implemented to simulate the free-cooling/heating mode of the ventilation system.

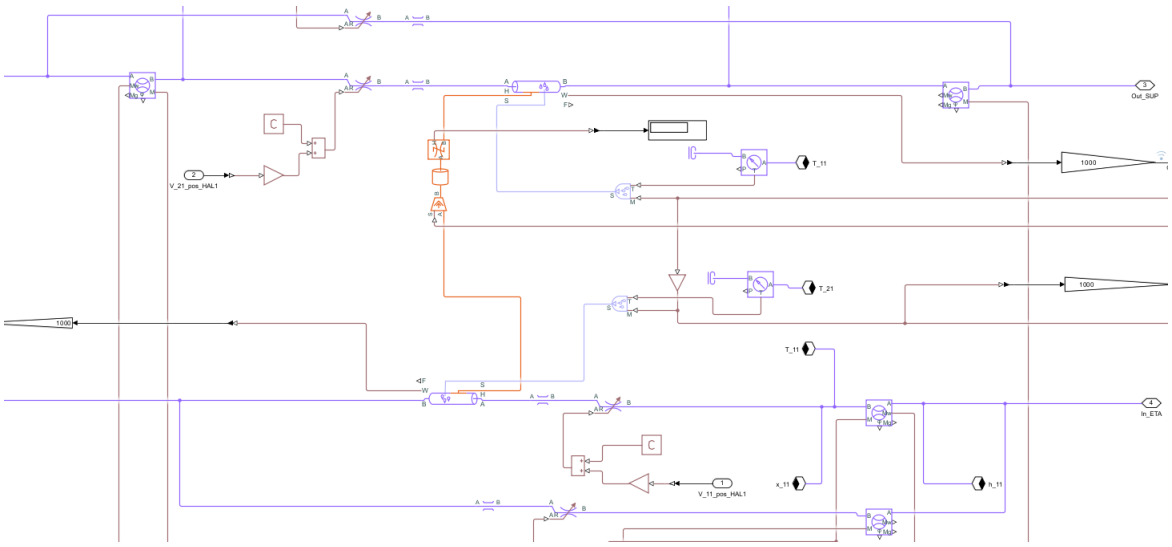

Figure 3. Simscape ERV/HRV exchanger model

To reduce the complexity of the modeling procedure, the aggregate heat transfer characteristics of the exchanger are derived by employing a single-channel analysis (as illustrated in Figure 4) with a counterflow model approach. Subsequently, these findings are extrapolated to encompass the entirety of the heat exchanger. The directional flow of heat and moisture is assumed to be positive, occurring from the extracted air (ETA) side to the supply air (SUP) side (control volume 3 to 1).

3.2.1. Sensible heat recovery Concerning the sensible heat recovered in the exchanger, the effectiveness-NTU method has been employed [2].

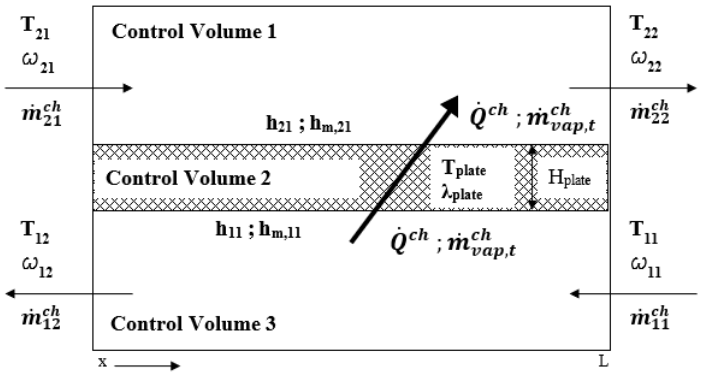

Figure 4. Counterflow model approach

The heat transfer rate exchanged between two channels ($\dot{Q}^{ch}$) is:

$$\dot{Q}^{ch} = \epsilon_s \dot{Q}^{ch}_{max} = \epsilon_s (\dot{m}^{ch} cp)_{min} (T_{11} - T_{21}) \qquad \epsilon_s = \frac{1 - e^{-NTU_s(1-C_r)}}{1 - C_r e^{-NTU_s(1-C_r)}} \tag{2}$$

where T_{11} denotes the inlet ETA flow temperature, T_{21} refers to the inlet SUP flow temperature, ϵ_s represents the sensible effectiveness for a counterflow type exchanger, $\dot{Q}^{ch}_{max}$ is the maximum recoverable heat flow rate per channel and $\dot{m}^{ch}_{11}$ and $\dot{m}^{ch}_{21}$ indicate the inlet mass flow rate per channel at the ETA side and SUP side, respectively.

The Number of Transferable Unit for sensible heat transfer (NTU_s) can be calculated as:

$$NTU_s = \frac{U_s A^{ch}}{C_{min}} \qquad U_s = (\frac{1}{h_{11}} + \frac{H_{plate}}{\lambda_{plate}} + \frac{1}{h_{21}})^{-1} \tag{3}$$

where:

- U_s is the global heat transfer coefficient;
- A^{ch} is the total heat transfer area per channel;
- h_{11} and h_{21} are the convective heat transfer coefficient for ETA and SUP side respectively;
- H_{plate} is the thickness of the membrane;
- λ_{plate} is the membrane thermal conductivity.

h_{11} and h_{21} can be calculated from the Nusselt Number:

$$h = \frac{Nu\lambda}{D_h} \tag{4}$$

λ is the air thermal conductivity for ETA and SUP flow respectively, and D_h is the hydraulic diameter of a single channel.

Considering the reduced dimension of the channels, for this type of exchangers, the fluid flow exhibits laminar characteristics (Reynolds number = 90 to 110), Consequently, the correlation established by Shah et al. [2] is employed to compute the Nusselt number in a rectangular of the heat exchangers.

$$Nu = 8.235[1 - 2.0421(\alpha^*) + 3.0853(\alpha^*)^2 - 2.4765(\alpha^*)^3 + 1.0578(\alpha^*)^4 - 0.1861(\alpha^*)^5] \tag{5}$$

The ratio between the two dimensions (a, b) of the channel cross-section is denoted as α^*. In this case a square channel is used, therefore $\alpha^* = \frac{a}{b} = 1$, the Nusselt number (Nu) is consequently equal to 3.608.

If we now consider the total number of channels per side ($n_{channel}$), it is possible to compute the overall heat exchange in the exchanger ($\dot{Q}$):

$$\dot{Q} = n_{channel}\dot{Q}^{ch} \tag{6}$$

In order to replicate the thermal inertia of the heat exchanger membrane and consequently achieve a more precise representation of thermal exchange during transitory conditions, a thermal mass has also been added into the model.

3.2.2. Latent heat recovery The equations for moisture recovery are derived mainly from the research conducted by Min et al. [5], Križo et al. [4] and Zhang et al. [9].

Similar to equation (2) it is feasible to define the moisture exchanged between two channels ($\dot{m}^{ch}_{vap,t}$) as:

$$\dot{m}^{ch}_{vap,t} = \epsilon_l(\dot{m}^{ch}_{dry})_{min}(\omega_{11} - \omega_{21}) \tag{7}$$

ω_{11} and ω_{21} indicate the humidity ratios of the two streams and $\dot{m}^{ch}_{dry}$ is the mass flow rate of dry air per channel. Consequently, the latent effectiveness (ϵ_l) can be computed as:

$$\epsilon_l = \frac{1 - e^{-NTU_l(1-R)}}{1 - Re^{-NTU_l(1-R)}} \qquad R = \frac{\dot{m}^{ch}_{min}}{\dot{m}^{ch}_{max}} \qquad NTU_l = \frac{U_l A^{ch}}{\dot{m}^{ch}_{min}} \tag{8}$$

The overall moisture transfer resistance (U_l) and the membrane permeability P_m can be calculated as follow:

$$U_l = \left(\frac{1}{h_{m,11}} + \frac{H_{plate}}{P_m} + \frac{1}{h_{m,21}}\right)^{-1} \qquad P_m = \frac{CD_{wm}\omega_{max}e^{5294/T}}{10^6(1 - C + \frac{C}{RH})^2 RH^2} \tag{9}$$

where D_{wm} the moisture diffusivity within the membrane, ω_{max} is the maximum moisture content of water vapor within the membrane, C rapresents the sorption curve shape and H_{plate} is the thickness of the membrane. To simplify the model, these properties were assumed to be constant and their values at 20°C were utilized, introducing a small margin of error. For equation (10), the temperature (T) and relative humidity (RH) were selected as the average values on the surface of the plate.

The convective moisture transfer coefficient h_m can be determined through the Chilton-Colburn analogy, employing the convective heat transfer coefficient, the Lewis number (Le, approximately 1.15 for air) [3], and the density ρ and specific heat capacity c_p of the stream.

$$h_m = \frac{h}{\mathrm{Le}^{2/3}\rho c_p} \tag{10}$$

In conclusion, the overall conveyed moisture is:

$$\dot{m}_{vap,t} = n_{channel}\dot{m}^{ch}_{vap,t} \tag{11}$$

3.2.3. Energy recovery exchanger model validation The validation experiments were conducted under the boundary conditions: $\mathrm{RH_{ODA}}$=82%, $\mathrm{T_{ODA}}$=2°C and $\mathrm{RH_{ETA}}$=61%, $\mathrm{T_{ETA}}$=20°C.

The experimental effectiveness values are computed as follows:

$$\epsilon_s = \frac{(\dot{m}c_p)_{21}(T_{22} - T_{21})}{(\dot{m}c_p)_{min}(T_{11} - T_{21})} \qquad \epsilon_l = \frac{(\dot{m})_{21}(\omega_{22} - \omega_{21})}{(\dot{m})_{min}(\omega_{11} - \omega_{21})} \tag{12}$$

Considering the results presented in Figure 5, Since the model error remains limited within the entire operating range of the system, the model can be considered validated.

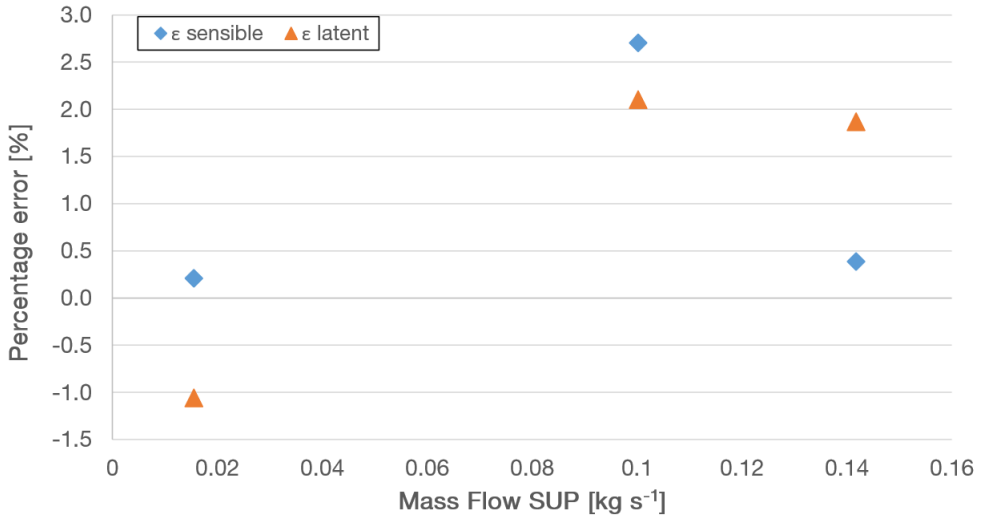

Figure 5. ERV model validation

3.3. Comparison between ERV and HRV

A concise comparison between the ERV and HRV heat recovery units can therefore be drawn. For this purpose two simulations were carried out and presented in Table 1:

Table 1. Comparison between ERV and HRV in terms of different transport variables.

ERV INPUT			**HRV INPUT**		
Volumetric flow rate	227	$m^3\ h^{-1}$	Volumetric flow rate	227	$m^3\ h^{-1}$
T_{ODA}	2	°C	T_{ODA}	2	°C
RH_{ODA}	50%		RH_{ODA}	50%	
T_{ETA}	20	°C	T_{ETA}	20	°C
RH_{ETA}	50%		RH_{ETA}	50%	
Humidity effectiveness	71%		Humidity effectiveness	0%	
Thermal effectiveness	83%		Thermal effectiveness	88%	
OUTPUT			**OUTPUT**		
Total (Enthalpy) effectiveness	79%		Total (Enthalpy) effectiveness	55%	
T_{SUP}	17	°C	T_{SUP}	17,92	°C
RH_{SUP}	48%		RH_{SUP}	17%	
T_{EHA}	5,9	°C	T_{EHA}	7,24	°C
RH_{EHA}	66%		RH_{EHA}	27,2%	
Humidity Transfer	0,27	$g\ s^{-1}$	Humidity Transfer	0	$g\ s^{-1}$
Water condensation in the exchanger	0	$g\ s^{-1}$	Water condensation in the exchanger	0,0765	$g\ s^{-1}$
Sensible Power Recovery	1147	W	Sensible Power Recovery	1219	W

The obvious advantage that immediately stands out is that the total effectiveness of the enthalpy exchange (ERV) is significant greater than that of the pure sensible exchanger (HRV). However, the latter has a more conductive membrane, which allows for higher outlet temperatures of the supply air (and therefore higher sensible effectiveness), although the result supplied air is drier. For a house with a high internal moisture production, it may be more convenient to use an HRV.

On the other hand, the HRV is more susceptible to the phenomenon of internal condensation, which in winter conditions can cause frosting on the exchanger. This should be prevented by inserting a pre-heater on the ODA channel, in order to avoid damaging the membrane of the exchanger and the inevitable decay of performance. The ERV, thanks to the transfer of humidity, allows for working with lower ODA temperatures without the risk of condensation and frosting.

This avoids the use of the pre-heater even with temperatures below 0°C, making the system more energy-efficient.

3.4. Aeraulic model calibration

The aeraulic model is fine-tuned based on experimental data obtained from a certified entity that conducted previous testing of the system. During the experiments, a volumetric flow rate of 227 m^3 h^{-1} was configured for both the extraction and supply airflow. The pressure losses across the external ducts were set at predetermined values, and the revolutions per minutes of the three fans were measured.

The same working conditions were then replicated on the model, and appropriate correction factors were found for the rotation speed of each fan to replicate the correct behavior of the system. Figure 6 shows the behavior of the OEA Fan, classified as a critical element of the system, after the calibration procedure:

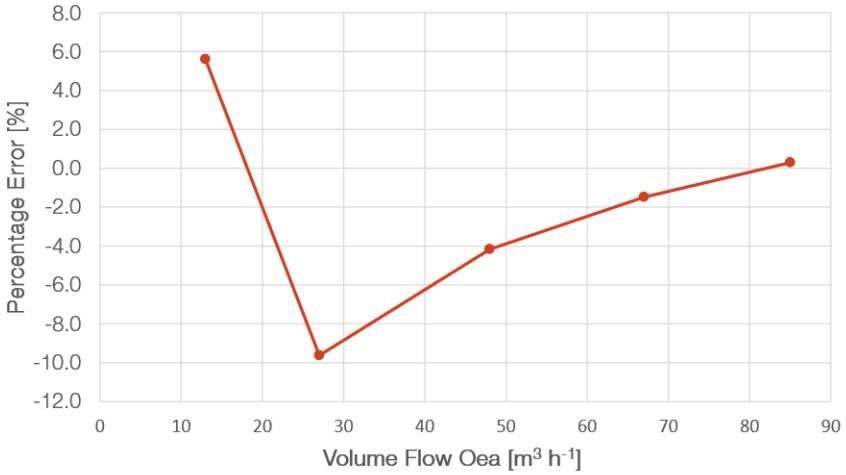

Figure 6. Model error

We adopted a calibration strategy based on the adjustment of fan characteristic curves instead of resistances. This approach was chosen considering the extensive number of flow resistances involved and the limited number of fans. By applying a correction factor of 160 rpm to the OEA fan, we achieved an accurate replication of the system's behavior. Similarly, the ETA fan required a correction factor of 245 rpm, while the SUP fan had an offset of 116 rpm. These compensatory offsets were introduced to mitigate some uncertainties in the system:

- The correction factor on the OEA fan mitigates the uncertainties of the ODA, OEA, and EHA branch flow resistances, including ODA filter, check valve, and T-junctions.
- Similarly, the correction factor on the ETA and SUP fans mitigate the uncertainties associated with the flow resistances in the ETA and SUP branches. Furthermore, it accounts for the uncertainties in the operating curves of the fans, which arise from the inclusion of a cochlea designed to optimize their performance.

The results presented in Figure 6 demonstrate a notable decrease in error as the flow rate increases. This phenomenon can be primarily attributed to the substantial deviation between the dimensionless operating curve and the actual operating fan curve at lower flow rates. In this particular scenario, measurements were intentionally conducted with elevated pressure losses in the external ducts to assess their impact on the OEA fan. As a result, the flow rate

remained predominantly small in most cases. However, it is important to note that under normal operating conditions, the system works at significantly higher flow rates. Therefore, considering the relatively low error observed at higher flow rates, the system can be deemed accurately calibrated with enough precision.

4. Results and discussion

4.1. Effect of installation conditions

The main emphasis of this paper is on the examination of the ventilation system and its performance. Nevertheless, a basic representation of the thermodynamic cycle of the heat pump is incorporated to achieve comprehensive physical modeling of the entire system and conduct sensitivity analyses. To maintain brevity, the details of the refrigeration model are omitted.

In this section, we evaluate the outcomes of the model through the assessment of various installation conditions:

Table 2. Installation conditions

	Installation		
	Ideal	**Medium**	**Critical**
ETA, SUP ducts lenght DN160 [m]	15	15	15
ODA, EHA ducts lenght DN200 [m]	1	0	0
ODA, EHA ducts lenght DN160 [m]	0	4	6
ETA, SUP number of bends 45°	2	4	6
ODA, EHA number of bends 45°	2	4	6
ETA, SUP Specific Flow Resistence [Pa s^2 kg^{-2}]	10434	11868	13302
ODA, EHA Specific Flow Resistence [Pa s^2 kg^{-2}]	721	5828	8462

The investigations were conducted during the winter season under the following conditions: $T_{ODA} = 2°C$, $RH_{ODA} = 50\%$, and the indoor parameters set to $T_{ETA} = 20°C$, $RH_{ETA} = 50\%$. The OEA fan operated at a speed of $n_{OEA} = 2500$ rpm, and the mass flow rates for both ETA and SUP sides were set to $\dot{m}_{ETA} = \dot{m}_{SUP} = 0.025$ kg s^{-1} (equivalent to approximately 75 m^3h^{-1}).

The three-fan system excels in providing high heat transfer rates even when the user requires reduced flow rates, for this reason a low supply mass flow rate was set.

Consider the compressor frequency of 45 Hz (fig. 7). It is evident that the presence of the OEA fan enhances the heat transfer rate by 32% compared to a conventional system in an ideal installation. This improvement is attributed to the increased flow rate at the evaporator. However, as the external pressure losses on the EHA and ODA channels increase, the heat transfer rate diminishes due to the limited rotation velocity (capped at 2500 rpm) of the OEA fan, enforced to minimize noise. Conversely, it has been established that increasing external pressure losses on the ETA and SUP channels solely affect the ETA and SUP fans, as they are not subjected to rotation velocity restrictions.

Furthermore, Figure 7 illustrates that the reduction in available heat transfer rate to the condenser intensifies as installation conditions worsen, particularly at higher compressor frequencies.

Another noteworthy analysis, entails investigating the influence of the OEA fan (and consequently, the installation) on the thermodynamic performance of the heat pump. In this scenario, the coefficient of performance (COP) solely pertains to the thermodynamic cycle.

In this case, a supply flow rate of $\dot{m}_{ETA} = \dot{m}_{SUP} = 0.0752$ kg s^{-1} (~ 227 m^3 h^{-1}) is imposed. From the results presented in Table 3, a minor reduction in the coefficient of performance (COP) is discerned as installation conditions are aggravated.

In conclusion, it is evident that the implementation of the three-fan system offers significant advantages in terms of system performance. However, meticulous attention must be given during

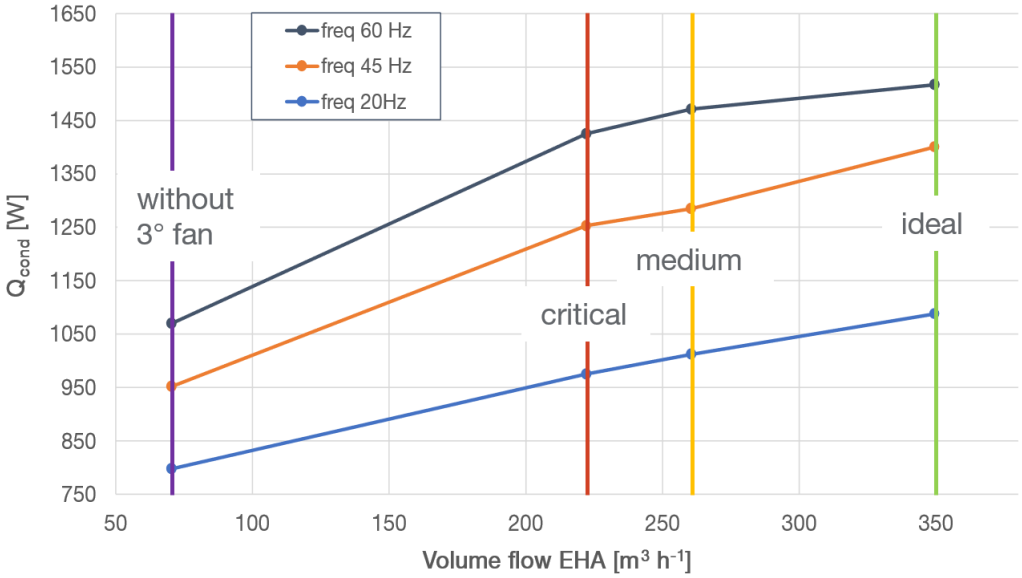

Figure 7. Condenser Heat transfer rate vs $\dot{V}_{EHA}$

Table 3. COP under different installation conditions

Installation	COP
ideal	7.30
medium	7.13
critic	7.07
without 3° fan	6.92

the installation phase to ensure proper realization of these advantages.

4.2. ODA Filter Fouling model

The investigation conducted in this section focuses on the fouling phenomenon occurring in the pre-filter situated within the ODA channel of the heat pump. The objective was to assess the impact of fouling on system performance in terms of the volumetric flow rate elaborated by the OEA fan. The boundary conditions were set to $T_{ODA} = 2°C$ and $RH_{ODA} = 50\%$. An ideal installation with a fixed fan rotation speed of $n_{OEA} = 2500$ rpm is assumed. The following assumptions were made regarding the fouling effects:

- The progression of pressure losses caused by filter fouling over time follows an exponential behaviour [10].
- The maximum allowable pressure drop is defined as three times the initial pressure drop of a clean filter [11].
- The analysis considers a time frame of 180 days starting from the installation of a new filter, during which fouling gradually accumulates until reaching the maximum acceptable level.

A comprehensive equation relating pressure drop and fouling for the examined filter can be formulated as follows:

$$\Delta p = R_{cleanfilter}(1 + e^{0.0294 \cdot d})\dot{m}^2 \tag{13}$$

where d represents the number of days elapsed since installation, and $e^{0.0294 \cdot d}$ represents the correction factor that captures the impact of filter fouling.

Table 4. Fouling degradation effect on $\dot{V}_{OEA}$

DAYS	Volume Flow OEA [m^3 h^{-1}]
0	233
90	232
120	231
180	221
220	198
250	156

Based on the analysis of the data presented in Table 4 (conducted with a volumetric flow rate of $\dot{V}_{SUP} = 227$ m^3 h^{-1}), it can be observed that over time, there is a noticeable decline in the flow rate elaborated by the third fan in the HP, resulting in a significant reduction in the available heat transfer rate at the evaporator. This decline, although not drastic, is still noteworthy when compared to the maximum expected performance. The underlying cause of this behavior is the initial pressure drop of the filter, which, despite being a coarse-mesh filter, remains relatively small even after being tripled at the 180th day. After the elapse of 180 days, the influence of

Table 5. $\dot{V}_{OEA}$ under different installation conditions

Installation	Volume Flow OEA [m^3 h^{-1}]
ideal	233
medium	139
critical	98.9
without 3° fan	0

filter fouling on system performance becomes markedly pronounced. A careful examination of the data presented in Table 4 and Table 5 highlights that, by the 250th day, the system operates almost akin to a medium-level installation, consequently yielding the anticipated repercussions outlined in the preceding section. It is, therefore, essential to strictly adhere to the regulatory recommendation of a maximum 180-day interval between filter replacements. Such adherence ensures the continual preservation of satisfactory system performance.

5. Conclusions and future developments

A lumped-parameters model of a ventilation system, coupled with a commercial heat pump, has been successfully devised and empirically calibrated. Specifically, an enthalpy recovery heat exchanger model was created using Simscape and verified through experiment. To assess the impact of incorrect installation and maintenance conditions, a refrigeration circuit was integrated into the system, allowing for an evaluation of the deteriorating effects on the overall thermodynamic cycle performance.

Further developments of the model will be executed and are possible in the future. These include: the calibration of the model regarding the refrigeration circuit, the thermal modeling of the building to which the system is coupled, and the precise implementation of the operating logic of the machine.

6. Acknowledgement
We express our sincere gratitude to the Zehnder Group - Competence Center Campogalliano (MO) for their invaluable assistance and the allocation of necessary resources throughout this research endeavor.

7. References
[1] Dorer V and Breer D 1998 *Energy Build.* **27** 247–255
[2] Shah R K and Sekulic D P 2003 *Fundamentals of heat exchanger design* (John Wiley & Sons)
[3] Min J and Su M 2010 *Appl. Therm. Eng.* **30** 991–997
[4] Križo K, Kapjor A and Holubčík M 2022 *Energies* **15** 6021
[5] Min J, Hu T and Liu X 2010 *J. Membr. Sci.* **357** 185–191
[6] Manz H, Huber H, Schälin A, Weber A, Ferrazzini M and Studer M 2000 *Energy Build.* **31** 37–47
[7] Filis V, Kolarik J and Smith K M 2021 *Energy Build.* **234** 110689
[8] MathWorks URL `https://it.mathworks.com/help/simscape/physical-modeling.html`
[9] Zhang L Z, Liang C H and Pei L X 2008 *J. Membr. Sci.* **325** 672–682
[10] Eker O F, Camci F and Jennions I K 2016 *MSSP* **75** 395–412
[11] 2017 UNI EN ISO 16890-1:2017 Filtri d'aria per ventilazione generale Standard